Investigation of dimensionality in superconducting NbN thin film samples with different thicknesses and NbTiN meander nanowire samples by measuring the upper critical field*

Mudassar Nazir[1,2], Xiaoyan Yang(杨晓燕)[3], Huanfang Tian(田焕芳)[1], Pengtao Song(宋鹏涛)[1,2], Zhan Wang(王战)[1,2], Zhongcheng Xiang(相忠诚)[1], Xueyi Guo(郭学仪)[1], Yirong Jin(金贻荣)[1], Lixing You(尤立星)[3], and Dongning Zheng(郑东宁)[1,2,4,†]

[1] *Institute of Physics and Beijing National Laboratory for Condensed Matter Physics, Chinese Academy of Sciences, Beijing* 100190, *China*
[2] *University of Chinese Academy of Sciences, Beijing* 100190, *China*
[3] *State Key Laboratory of Functional Materials for Informatics, Shanghai Institute of Microsystem and Information Technology and the Center for Excellence in Superconducting Electronics, Chinese Academy of Sciences, Shanghai* 200050, *China*
[4] *Songshan Lake Materials Laboratory, Dongguan* 523808, *China*

(Received 30 April 2020; revised manuscript received 27 May 2020; accepted manuscript online 28 May 2020)

We study superconducting properties of NbN thin film samples with different thicknesses and an ultra-thin NbTiN meander nanowire sample. For the ultra-thin samples, we found that the temperature dependence of upper critical field (H_{c2}) in parallel to surface orientation shows bending curvature close to critical temperature T_c, suggesting a two-dimensional (2D) nature of the samples. The 2D behavior is further supported by the angular dependence measurements of H_{c2} for the thinnest samples. The temperature dependence of parallel upper critical field for the thick films could be described by a model based on the anisotropic Ginzburg–Landau theory. Interestingly, the results measured in the field perpendicular to the film surface orientation show a similar bending curvature but in a much narrow temperature region close to T_c for the ultra-thin samples. We suggest that this feature could be due to suppression of pair-breaking caused by local in-homogeneity. We further propose the temperature dependence of perpendicular H_{c2} as a measure of uniformity of superconducting ultra-thin films. For the thick samples, we find that H_{c2} shows maxima for both parallel and perpendicular orientations. The H_{c2} peak for the perpendicular orientation is believed to be due to the columnar structure formed during the growth of the thick films. The presence of columnar structure is confirmed by transmission electron microscopy (TEM). In addition, we have measured the angular dependence of magneto-resistance, and the results are consistent with the H_{c2} data.

Keywords: NbN micro-bridges and NbTiN meander nanowire, upper critical field, low dimensionality, anisotropic magneto-resistance

PACS: 81.16.Rf, 74.78.–w, 74.25.–q, 74.25.F– **DOI:** 10.1088/1674-1056/ab9740

1. Introduction

Superconducting NbN material is of considerable interest for various kinds of applications. The upper critical field of this material can exceed 50 T and the transition temperature T_c is above 15 K.[1–3] Over the past fifteen years, meander nanowires made from ultra-thin films show great potential for single photon detections.[4–6] The devices are normally current biased and operate in the region very close to superconducting-resistive transition. The superconducting nature of the ultra-thin films or nanowires could affect the device performance greatly. For instance, the critical fields and critical current dependence on temperature could be substantially different for ultra-thin films whose dimensionality could be a 2D nature instead of 3D nature as in the case of bulks or thick films, depending on the ratio of film size to basic parameters such as the superconducting coherence length or the penetration depth. When the film thickness is comparable to the superconducting coherence length, it leads to the emergence of several interesting phenomena absent in the bulk form. For example, enhanced upper critical field, BKT transition, proximity effect, and dimensional crossovers have been reported.[7–19] The exact nature and the visibility of emergent dimensional phenomena below T_c depend on the thickness of the films and the coherence length normal to the film surface.

In this work, we investigate the dimensionality and anisotropic properties of superconducting NbN thin film samples by measuring the upper critical field on samples with different thickness. The NbTiN meander nanowire sample is also studied. We analyze the temperature dependence data together with the angular dependence of H_{c2} results to study the dimensionality of the samples. For the ultra-thin samples, when measured in field parallel to film surface orientation, we observe an upturn curved temperature dependence of H_{c2}, indicating that the samples are in the 2D regime. This is further supported by the angular dependence data that show H_{c2} following a 2D angular dependence relation. In the case of field perpendicular to

*Project supported by the Chinese Academy of Sciences (Grant No. XDB25000000).
†Corresponding author. E-mail: dzheng@iphy.ac.cn

the film surface, the linear temperature dependence, expected from the Ginzburg–Landau theory, is observed in most samples, except for ultra-thin 4 nm NbN film and NbTiN nanowire samples. On the ultra-thin samples, we observe curved temperature dependence of H_{c2}. We interpret this phenomenon based on a model considering local in-homogeneity caused suppression of pair-breaking.[20] Additionally, we also perform magneto-resistance measurements as a function of angles between the applied field and film surface on the samples. The angular dependence of magneto-resistance appears to be consistent with the H_{c2} data. For the thick samples, the parallel and perpendicular upper critical field curves crisscross each other, indicating enhanced H_{c2} in the perpendicular orientation. We discuss this effect by considering the columnar structures observed in the thick films.

2. Experimental details

NbN thin films of different thickness 4–100 nm were deposited on thermally oxidized Si (100) substrates by means of direct current (DC) reactive magnetron sputtering at room temperature. The substrates are 10 mm×10 mm in size and 500 μm in thickness. The base pressure of the deposition chamber was maintained at a level lower than 5.5×10^{-8} Pa before sputtering in the mixture of high purity Ar and N_2 gas. The Nb target had a purity of better than 99.95%. N_2 gas flowed into the chamber to a required pressure. After that, high purity Ar gas (99.999%) was supplied until the required total pressure was reached. In order to prevent active gas contamination, the Ar gas was supplied through a customized built-in non-evaporable getter (NEG) purifier before flowing into the sputtering chamber. The x-ray diffraction (XRD) and x-ray reflectivity (XRR) characterization of the thin film samples were performed to determine the sample quality and film thickness. For electrical transport measurements, the NbN thin films of different thicknesses 4 nm, 20 nm, 50 nm, and 100 nm were patterned into micro-bridges of 20 μm width and 1000 μm length connected with four pads by using photolithography and reactive ion etching (RIE) based on Ar/SF_6 gas mixture and lift off process. The NbTiN meander nanowire with 70 nm width and 500 μm length for single photon detector based on 5 nm thickness film was fabricated by electron beam lithography (EBL) process.[21]

Transport measurements were carried out in a Quantum Design physical properties measurement system (PPMS) with the highest magnetic field up to 9 T and the lowest temperature down to 2 K.

3. Results and discussion

3.1. X-ray diffraction

The XRD pattern measured for orientation analysis of the NbN thin film is given in Fig. 1. The result shows that the (111) diffraction peak is from the NbN thin film and (100) is from the silicon (Si) substrate. The film thickness was determined by XRR measurements and the results are presented in Fig. 2. The XRR results for different thickness NbN films with about 0.5 nm surface roughness were deduced from a multilayer model by fitting the XRR data.

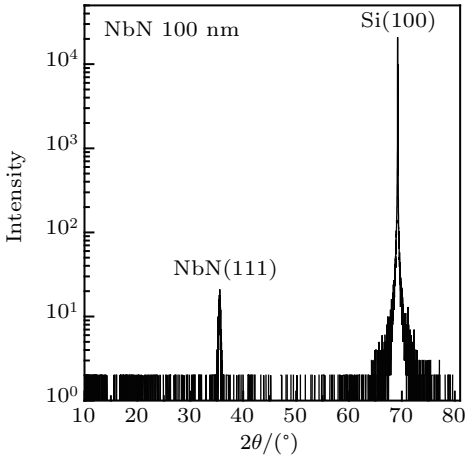

Fig. 1. XRD characterization of NbN 100 nm thin film.

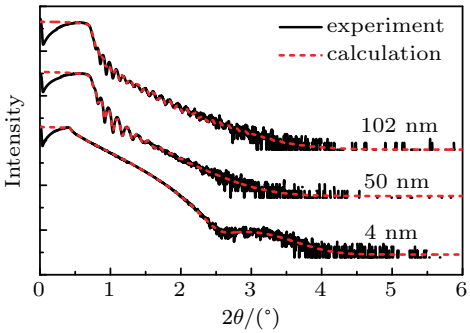

Fig. 2. XRR measurements were performed on NbN films of given thicknesses. Experimental results (black solid line) of the specimens were fitted (red short dash) by a multilayer model from bottom to top with the fitted NbN thicknesses shown.

3.2. Thickness dependence of T_c

The resistive transition curves under zero magnetic field for different thickness micro-bridges measured from 2 K to 300 K are illustrated in Fig. 3(a). The results show that superconducting transition temperature T_c decreases with decreasing thickness and the thickness dependence of T_c is shown in Fig. 3(b).

The suppression of T_c with decreasing thickness in the superconducting films is in agreement with previous reports.[10,17,22–25] This fall of T_c is a dimensional crossover phenomenon driven by the strength of the order parameter fluctuations, which increases with reduced dimensionality.[26]

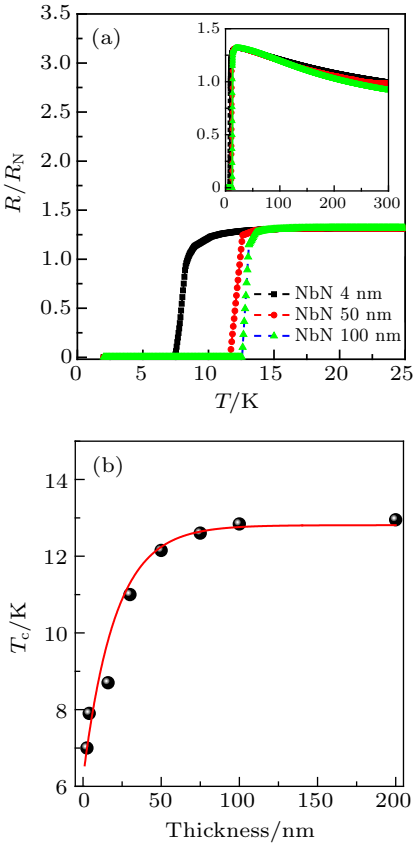

Fig. 3. (a) Normalization of resistance as a function of temperature curves for different micro-bridges at zero fields. Inset: R–T is measured from 2 K to 300 K. (b) Thickness dependence of the transition temperature. The black solid symbols are experimental data and the red solid line is to guide the eyes.

3.3. Temperature dependence of H_{c2} for different thicknesses

Resistive transition $R(T,H)$ curves under different applied magnetic fields in both the parallel and perpendicular orientations of the superconducting specimens are displayed in Fig. 4 for three samples. As expected, the transition curves shift towards lower temperature with increasing magnetic field apparently, which do not broaden significantly in both parallel and perpendicular directions for the all given samples. To evaluate the superconducting behavior, we analyze the temperature dependence of the upper critical field for different thickness specimens. The upper critical field H_{c2} is defined at half of the residual resistance ($R_{15\ \mathrm{K}}$ = residual resistance), the data are shown in Fig. 5 for three NbN samples and one NbTiN sample, respectively.

From these results, several features of $H_{c2}(t)$ could be identified. Firstly, all samples show clearly anisotropy in the upper critical field. In other words, the difference between $H_{c2\perp}(t)$ and $H_{c2||}(t)$ is substantial. Secondly, the $H_{c2||}(t)$ curves show upturn bent curvatures, especially at temperatures close to T_c. This feature is more pronounced for the ultra-thin samples. In contrast, the $H_{c2\perp}(t)$ curves show mostly linear behavior, except for the very thin ones. Thirdly, for the two thicker samples (50 nm and 100 nm), the $H_{c2\perp}(t)$ and $H_{c2||}(t)$ curves show crisscross as exhibited in Figs. 5(b) and 5(c).

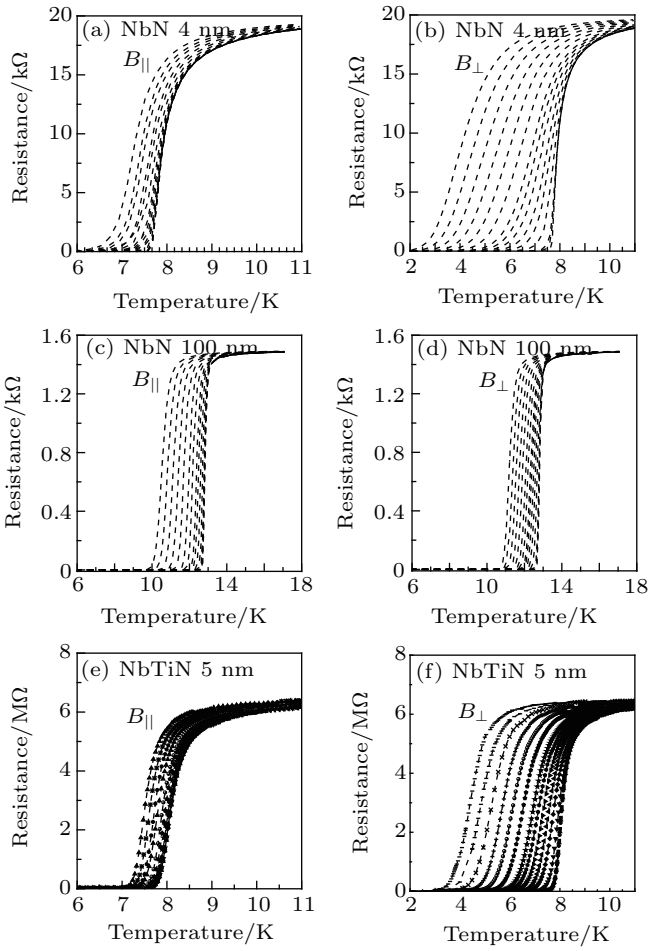

Fig. 4. The R–T curves measured in different applied magnetic fields 0, 0.05, 0.1, 0.5, 1, 1.5, 2, 2.5, 3, 3.5, 4, 4.5, 5, 6, 7, 8, 9 (right to left, in units of T) for given specimens in both parallel and perpendicular orientations. By increasing the field, all curves move towards lower temperatures apparently and do not broaden.

We first discuss the bent curvature of $H_{c2||}(t)$ for samples with different thicknesses. This kind of feature has been widely observed in ultra-thin superconducting films[20,27–31] and is explained by the 2D nature of the films when the film thickness becomes smaller than the superconducting coherence length of the material.[32] Harper and Tinkham have solved the linearized Ginzburg–Landau equation under the limit $d \ll \xi$[33] and obtained

$$H_{c2||}(t) = \frac{\sqrt{3}\Phi_0}{\pi d \xi_{||}(0)}(1-t)^{1/2}, \tag{1}$$

where Φ_0 is the flux quantum 2.07×10^{-15} wb, $t = T/T_c$, and d is the thickness of the specimens. The curved behavior of the parallel upper critical fields follows Eq. (1) as represented with the blue dash line in Figs. 5(a)–5(c) in the limit $d < \xi$ which extracts the 2D behavior in the presented samples. The coherence length increases with increasing temperature and diverges close to T_c, the 2D region is more pronounced for ultra thin samples and moves towards T_c with increasing thickness as presented in Figs. 5(a)–5(c).

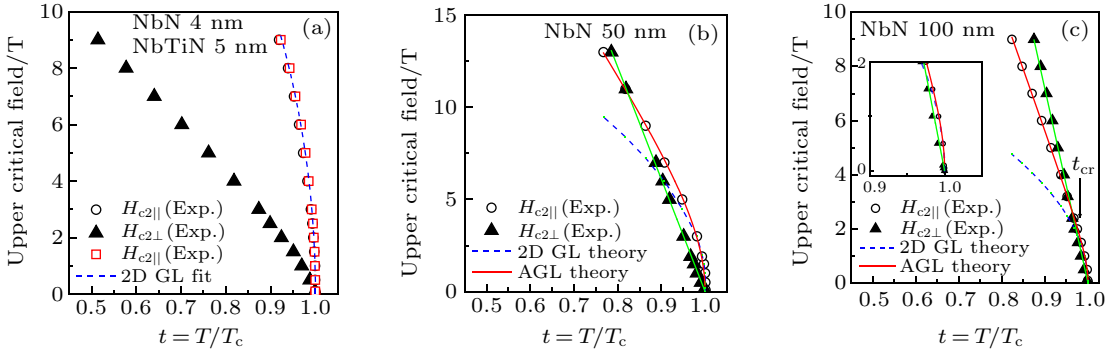

Fig. 5. The temperature dependent parallel and perpendicular upper critical field diagrams. (a) The upper critical field for ultra thin 4 nm film and NbTiN 5 nm nanowire. The $H_{c2||}(t)$ shows pronounced 2D behavior and is well fitted with 2D GL Eq. (1) as indicated by the blue dash line. The black open circles and red open squares represent $H_{c2||}(t)$ for 4 nm NbN film and NbTiN 5 nm wire, respectively, and the $H_{c2||}(t)$ dependence shows a similar behavior. The solid triangles illustrate the $H_{c2\perp}(t)$ data for NbN 4 nm film. (b), (c) The parallel critical field decreases while the perpendicular upper critical field rises with increasing thickness and the bending curvature moves towards T_c. The $H_{c2||}(t)$ is explained with AGL interpolation crossover Eq. (2) and the perpendicular upper critical field data exhibit a linear behavior and are well fitted with Eq. (3). The arrows show t_{cr} crossover temperature, and $H_{c2}(t)$ shows crisscross in high thickness samples. The open circles and solid triangles represent parallel and perpendicular field experimental data, respectively, and are fitted using Eqs. (2) and (3) as shown by the red and green solid lines.

As d starts to increase and becomes comparable or even larger than the coherence length $d > \xi$, the system undergoes a crossover to a 3D linear region, which is clearly observed for the thick film samples. Schneider and Locquet have investigated crossover using the linearized AGL theory[26] and obtained an expression for a large temperature region that covers the crossover

$$H_{c2||}(t) = \frac{\Phi_0}{2d\xi_{||}(0)}\left(\frac{1}{1-t} + \frac{d^2}{\pi^2(\xi_\perp(0))^2}\right)^{1/2}(1-t). \quad (2)$$

Here, $\xi_{||}(0)$ and $\xi_\perp(0)$ represent the parallel and perpendicular coherence lengths, respectively. Clearly, the equation gives linear and parabolic temperature dependences of $H_{c2||}$ in the limiting cases of $d \ll \xi$ and $d \gg \xi$, respectively.

The temperature dependence of the perpendicular upper critical field $H_{c2\perp}$ shows a linear behavior for the thick samples as predicated by the Ginzburg–Landau theory. However, we note that the ultra-thin samples and the NbTiN nanowire sample show slightly upturn curvatures in $H_{c2\perp}(t)$. The somewhat unexpected results will be discussed in Subsection 3.4.

The linear temperature dependence of the perpendicular upper critical field is given[26] as

$$H_{c2\perp}(t) = \frac{\Phi_0}{2\pi(\xi_{||}(0))^2}(1-t). \quad (3)$$

We may estimate the parallel coherence length by fitting $H_{c2\perp}(t)$ data using Eq. (3) for the thick films as indicated by the green solid lines in Figs. 5(b) and 5(c). The $\xi_{||}$ (0) and d are then used to fit the $H_{c2||}(t)$ data using Eq. (2), the best fit $H_{c2||}(t)$ data estimates the $\xi_\perp(0)$ values. The estimated values are given in Table 1. The crossover temperatures are marked as arrows. The values of ξ (0) in either field direction for our NbN micro-bridges are comparable to those reported for similar width films in literature,[27] which are 6.0–9.4 nm[34] and 1.6–4.0 nm,[35,36] respectively.

Table 1. The parameters, coherence lengths, and T_c defined at half of residual resistance for given samples.

Sample	T_c/K	$\xi_{||}(0)$/nm	$\xi_\perp(0)$/nm
NbTiN 5 nm wire	8.1	6.46	
NbN 4 nm	7.9	8.6	
NbN 50 nm	12.42	2	5
NbN 100 nm	12.83	2.14	7

3.4. Nonlinear behavior of $H_{c2\perp}$ for ultra thin samples

Interestingly, the temperature dependence of the perpendicular upper critical field exhibits a bending curvature very close to T_c in ultra thin NbN and NbTiN meander nanowire samples as shown in Fig. 6. This behavior was also reported previously.[20,28,30] In Ref. [24], it was suggested that the observed upturn bending in Nb meander nanowire samples could be due to the dimensional crossover effect when the coherence length $\xi_{||}$ becomes larger than the width of the nanowire samples. Although this is a possible scenario because the coherence length diverges at T_c, it should only appear at a temperature region very close to T_c. Further, in this case of study, the width of the NbN samples is 20 μm that suggests the dimensional crossover effect can hardly be seen. Alternatively, Nam *et al.* have investigated the critical field of a superconducting nanomesh network.[20] They found a similar upturn curvature in the temperature dependence of the perpendicular critical field for the samples which were not fully covered by superconducting grains while a linear behavior was observed for the fully covered ultra-thin film samples. They suggested that the local variation in T_c led to suppression of pair-breaking and, hence, enhanced the critical field near T_c.

We may use this model to explain our $H_{c2\perp}$ data for the ultra-thin samples. In these samples, there could be a local small variation in T_c. Furthermore, when we compare the 4 nm NbN sample to the NbTiN nanowire sample, we note that the former shows more clear upturn curvature in $H_{c2\perp}(t)$. This indicates that the 4 nm NbN sample may have larger lo-

cal variation in T_c than the NbTiN nanowire sample, being in agreement with the in-field transition data measured on the two samples, as shown in Figs. 4(b) and 6(a).

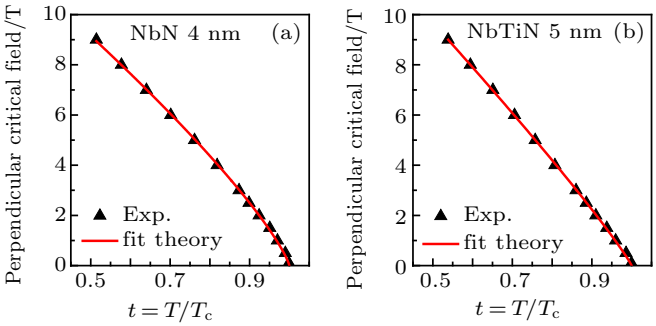

Fig. 6. Temperature dependence of the perpendicular upper critical field results for the ultra-thin NbN and the NbTiN nanowire samples. Bending curvature close to T_c is observed and the red solid lines are the fitted curves using a $(1-t)^{\gamma}$ relation.

Empirically, we could fit the $H_{c2\perp}(t)$ data using $(1-t)^{\gamma}$ relation with γ as a fitting parameter. The perpendicular upper critical field data is fitted and indicated with a red solid line in Figs. 6(a) and 6(b) for the ultra thin NbN and NbTiN nanowire samples, the best fits give $\gamma = 0.8$ and 0.9 for these two samples, respectively.

Based on the results, we propose that we may use the temperature dependence of $H_{c2\perp}$ as a measure of uniformity of superconducting ultra-thin films. In other words, a linear behavior of $H_{c2\perp}(t)$ could be an indication of better quality for ultra-thin samples.

3.5. Angular dependence of H_{c2}

In order to clarify the 2D behavior of the 4 nm thin NbN film and 5 nm thick NbTiN nanowire samples, angular dependent upper critical field measurements were performed on these two samples. The measurements were carried out at fixed temperatures close to T_c and at different angles by sweeping the magnetic field up to 9 T. The results are shown in Figs. 7(a) and 7(b), where θ is the angle between the normal of the sample plane and the direction of the applied magnetic field. The angles 0° and 90° are defined as perpendicular and parallel directions to the surface of the samples. We choose the upper critical field at half of the residual resistance and draw H_{c2} vs. θ graph. The results are presented in Figs. 7(c) and 7(d).

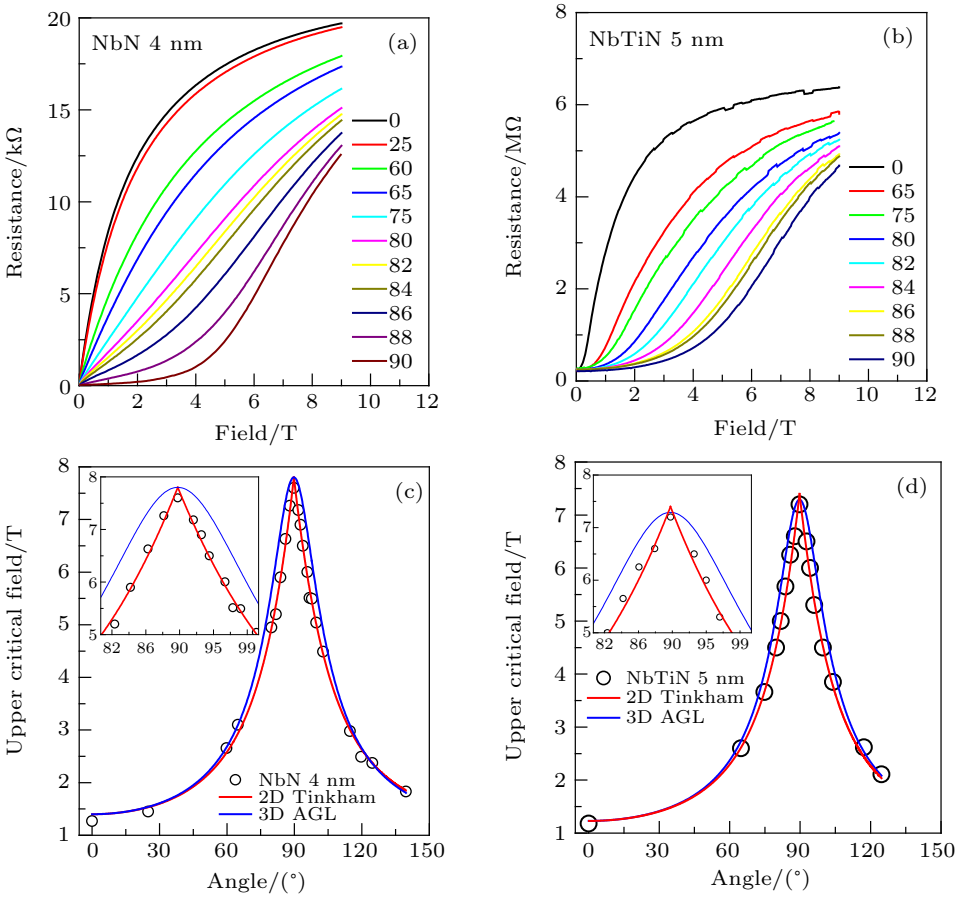

Fig. 7. Superconducting resistive transition curves under applied magnetic field 0 up to 9 T at different angles for (a) NbN 4 nm at temperature 7.8 K and (b) NbTiN 5 nm at 7.8 K. The upper critical field is defined at half of residual resistance and its angular dependence is shown for (c) NbN 4 nm and (d) NbTiN 5 nm nanowire. The sharp peak is seen at $\theta = 90°$ for given samples which is fitted with the 2D Tinkham and 3D anisotropic formulas given in Eqs. (4) and (5) as indicated by the red and blue solid lines, respectively. The black circles represent the experimental data. The inset shows a zoom-in view of the region around $\theta = 90°$.

It is well known that a 2D superconductor and an anisotropic 3D superconductor show different angular dependences of H_{c2}.[37–39] In the 2D case, H_{c2} (θ) follows the 2D Tinkham model given as

$$\left|\frac{H_{c2}(\theta)\cos(\theta)}{H_{c2\perp}}\right| + \left(\frac{H_{c2}(\theta)\sin(\theta)}{H_{c2||}}\right)^2 = 1, \quad (4)$$

while in the anisotropic 3D case, the following relation[40] applies:

$$\left(\frac{H_{c2}(\theta)\cos(\theta)}{H_{c2\perp}}\right)^2 + \left(\frac{H_{c2}(\theta)\sin(\theta)}{H_{c2||}}\right)^2 = 1. \quad (5)$$

The key feature that characterizes the difference between the two cases is the shape of H_{c2} (θ) around the direction with the field parallel to the sample surface. The 2D model shows a cusp-like peak, while the 3D model presents a round maximum.

In our samples, a cusp like peak is clearly observed at $\theta = 90^\circ$ where the external magnetic field is aligned in parallel to the sample surface, as shown in Fig. 7. The red and blue solid lines represent fitting results using Eqs. (4) and (5) for 2D and 3D systems, respectively. These results suggest that the ultra-thin NbN and NbTiN nanowire samples are in the 2D regime as we have discussed in Subsection 3.3.

3.6. Enhanced $H_{c2\perp}$ in thick NbN film samples

As shown in Fig. 5(c), the parallel and perpendicular upper critical field curves of the 100 nm NbN sample crisscross each other at a certain temperature. Below the crisscross, $H_{c2||}$ is higher than $H_{c2\perp}$ and above the crisscross point at low temperature, it exhibits the opposite behavior. The similar behavior is also observed for the NbN 50 nm sample. Interestingly, the crisscross is found to shift toward T_c with increasing thickness. This shift of crisscross can be understood by considering the much reduced 2D region in the thicker sample.

The existence of the crisscross also indicates that $H_{c2\perp}$ would show maxima in the angular dependence of the upper critical field. In Fig. 8(a), we present data for the 100 nm sample. Indeed, the upper critical field not only shows a peak in the parallel orientation, but also exhibits maxima in the perpendicular direction. In this case, $H_{c2\perp}$ is even higher than $H_{c2||}$.

The enhanced upper critical field in the perpendicular direction has been reported before in NbN films and is related to the columnar structures formed during the film growth.[35] We checked microstructure of the 100 nm sample using the transmission electron microscopy (TEM), the results are shown in Fig. 8(b). From the TEM micrographs, columnar-like structures along the direction normal to the sample surface can be seen clearly with a typical size around 5 nm. The presence of the columnar structures could reduce the mean free path and, thus, reduce the effective in-plane coherence length, leading to enhancement of $H_{c2\perp}$.

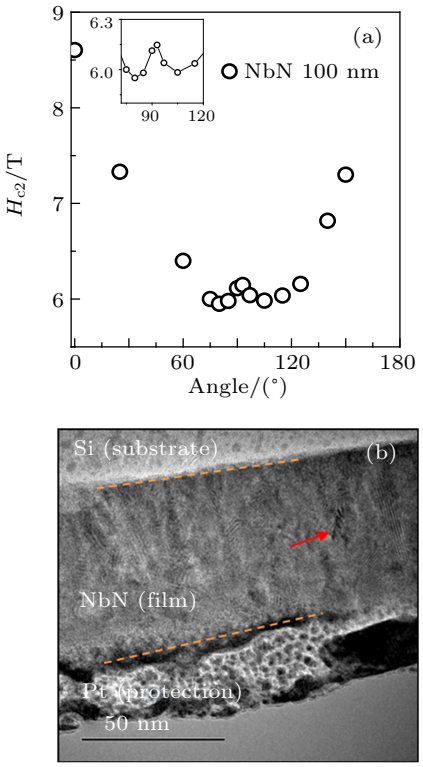

Fig. 8. (a) Angular dependence of upper critical field graph for NbN 100 nm is taken at temperature 11.25 K. The upper critical field shows maxima for both parallel and perpendicular orientations. The H_{c2} peak for the perpendicular orientation is believed to be due to the columnar structures formed during the growth of the thick films. (b) TEM image clearly shows columnar in NbN 100 nm film. The top, middle, and bottom layers represent the substrate, film, and protection layer, respectively. The red arrow indicates the one typical columnar structure.

3.7. Angular dependence of magneto-resistance

To further investigate the anisotropic properties of the samples, we carried out angular dependent magneto-resistance measurements at different temperatures and at fixed field 5 T. During the measurement, the sample was rotated along the axis perpendicular to the magnetic field and the current was also applied in the rotating axis direction. The results are shown in Fig. 9 for two samples, 4 nm and 100 nm NbN films. The angular dependence of the magneto-resistance is also obtained for the NbTiN nanowire sample, and the result is similar to that of the 4 nm NbN sample. The anisotropic magneto resistance (AMR) is observed. Within a full rotation, two minima appear in the AMR data of the 4 nm NbN sample and four minima are observed for the thick 100 nm NbN sample. Bearing in mind that the angular dependence of the magneto-resistance is controlled by the angular variation of H_{c2}, the results are consistent with the previous temperature and angular dependent upper critical field data. The extra minima observed in the 100 nm sample are due to the columnar structure, as we discussed in the previous subsection.

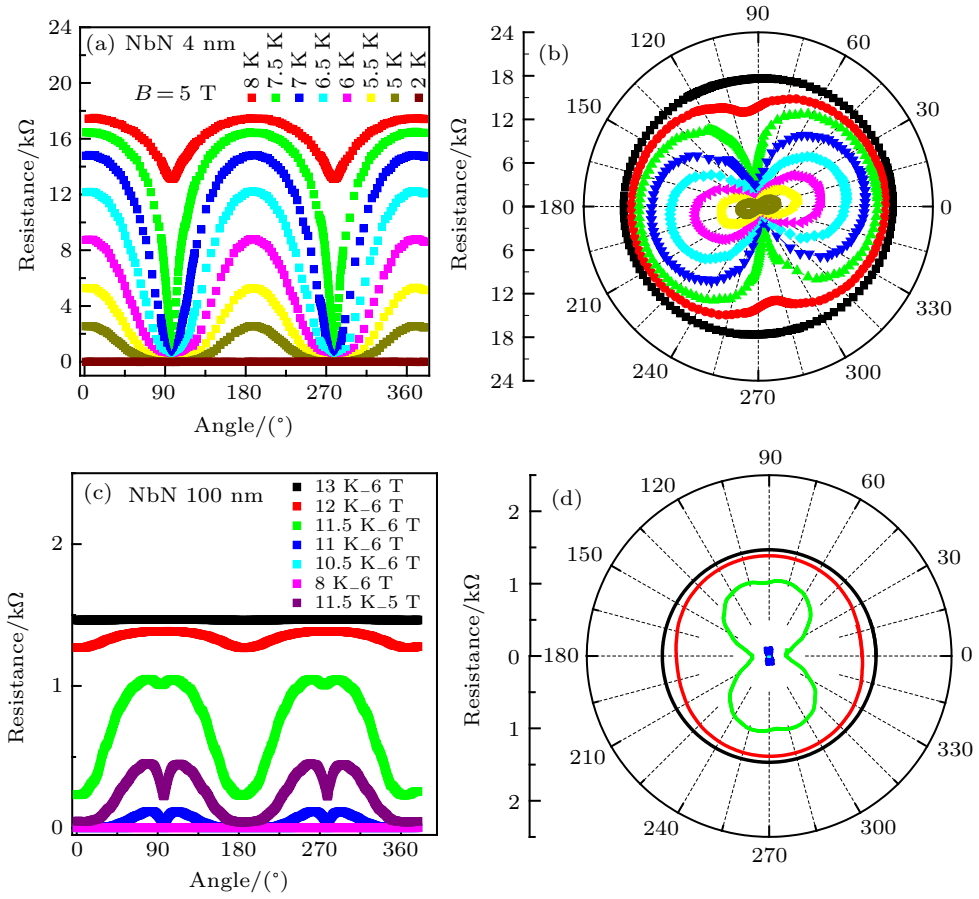

Fig. 9. (a), (c) Angular variation of the resistance for NbN 4 nm thin and 100 nm thick films at fixed applied field for different temperatures. (b), (d) Polar plot of magneto-resistance is observed folding symmetry.

4. Conclusion

Superconducting characteristics of NbN thin films with different thicknesses have been studied together with NbTiN meander nanowire samples. Temperature and angular dependences of the upper critical field are measured. The parallel upper critical field $H_{c2||}$ shows 2D behavior and is more pronounced for the ultra thin samples. Temperature dependence of the perpendicular upper critical field for the thick samples shows a linear behavior while the ultra thin samples exhibit a bending curvature close to T_c. The bending curvature of $H_{c2\perp}$ is explained by the suppression of orbital pair breaking effect caused presumably by local in-homogeneity. We suggest that one may use the temperature dependence of $H_{c2\perp}$ as a possible way for observing the quality of ultra-thin films. Further, dimensional behavior is confirmed by angular dependence of the upper critical field close to T_c that is well fitted with 2D Tinkham model for given samples. For the thick samples, we find that H_{c2} shows maximum for both parallel and perpendicular orientations. The H_{c2} peak for the perpendicular orientation is believed to be due to the columnar structures formed during the growth of the thick films. The presence of columnar structures is confirmed by transmission electron microscopy. Further, we measure the anisotropic magneto-resistance. The data are consistent with the upper critical field data.

Acknowledgement

The authors thank Zhang Y Z for technical assistance with PPMS.

References

[1] Jha R, Kumar A and Awana V P S 2012 *AIP Conf. Proc.* **1447** 867
[2] Vasyutin M A, Kuz'michev N D and Shilkin D A 2016 *Phys. Solid State* **58** 236
[3] Hazra D, Tsavdaris N, Jebari S, Grimm A, Blanchet F, Mercier F, Blanquet E, Chapelier C and Hofheinz M 2016 *Supercond. Sci. Technol.* **29** 105011
[4] Zhang C, Zhang W, Huang J, You L, Li H, Lv C, Sugihara T, Watanabe M, Zhou H, Wang Z and Xie X 2019 *AIP Adv.* **9** 075214
[5] Zhang W, You L, Li H, Huang J, Lv C, Zhang L, Liu X, Wu J, Wang Z and Xie X 2017 *Sci. Chin. Phys. Mech. & Astron.* **60** 120314
[6] Liu J, Zhang L Q, Jiang Z N *et al*. 2016 *Chin. Phys. Lett.* **33** 088502
[7] Zhao W, Wang Q, Liu M, Zhang W, Wang Y, Chen M, Guo Y, He K, Chen X, Wang Y, Wang J, Xie X, Niu Q, Wang L, Ma X, Jain J K, Chan M H W and Xue Q K 2013 *Solid State Commun.* **165** 59
[8] Matsuda Y, Komiyama S, Onogi T, Terashima T, Shimura K and Bando Y 1993 *Phys. Rev. B* **48** 10498
[9] Inoue M, Matsushita H, Hayakawa H and Ohbayashi K 1995 *Phys. Rev. B* **51** 15448
[10] Fàbrega L, Camón A, Fernández-Martínez I, Sesé J, Parra-Borderías M, Gil O, González-Arrabal R, Costa-Krämer J L and Briones F 2011 *Supercond. Sci. Technol.* **24** 075014
[11] Chun C S L, Zheng G G, Vincent J L and Schuller I K 1984 *Phys. Rev. B* **29** 4915
[12] Wong H K and Ketterson J B 1986 *J. Low Temp. Phys.* **63** 139
[13] Locquet J P, Neerinck D, Vanderstraeten H, Sevenhans W, Haesendonck C V, Bruynseraede Y, Homma H and Schuller I K 1987 *Jap. J. Appl. Phys.* **26** 1431

[14] Gao Z X, Osquiguil E, Maenhoudt M, Wuyts B, Libbrecht S and Bruynseraede Y 1993 *Phys. Rev. Lett.* **71** 3210
[15] Armenio A A, Cirillo C, Iannone G, Prischepa S L and Attanasio C 2007 *Phys. Rev. B* **76** 024515
[16] Gupta A, Singh G, Kumar D, Kishan H and Budhani R C 2013 *Appl. Phys. Lett.* **103** 182602
[17] Bo H, Ren T, Chen Z *et al*. 2019 *Chin. Phys. B* **28** 067402
[18] Gong X X, He X Z, Peng C X, *et al.* 2015 *Chin. Phys. Lett.* **32** 067402
[19] Zhang W H, Sun Y, Zhang J S *et al*. 2014 *Chin. Phys. Lett.* **31** 017401
[20] Nam H, Chen H, Adams P W, Guan S Y, Chuang T M, Chang C S, MacDonald A H and Shih C K 2018 *Nat. Coms.* **9** 5431
[21] Yang X, You L, Zhang L, Lv C, Li H, Liu X, Zhou H and Wang Z 2018 *IEEE Trans. Appl. Supercond.* **28** 1
[22] Naugle D G, Glover R E and Moormann W 1971 *Physica* **55** 250
[23] Quateman J H 1986 *Phys. Rev. B* **34** 1948
[24] Minhaj M S M, Meepagala S, Chen J T and Wenger L E 1994 *Phys. Rev. B* **49** 15235
[25] Bose S, Raychaudhuri P, Banerjee R, Vasa P and Ayyub P 2005 *Phys. Rev. Lett.* **95** 147003
[26] Schneider T and Locquet J P 1991 *Phys. C: Supercond.* **179** 125
[27] Joshi L M, Verma A, Rout P K, Kaur M, Gupta A and Budhani R C 2017 *Phys. C: Supercond. Its Appl.* **542** 12
[28] Zhao L, Jin Y R, Li J, Deng H and Zheng D N 2014 *Chin. Phys. B* **23** 087402
[29] Broussard P 2017 *J. Low Temp. Phys.* **189** 108
[30] Haberkorn N, Zhang Y Y, Kim J, McCleskey T M, Burrell A K, Depaula R F, Tajima T, Jia Q X and Civale L 2013 *Supercond. Sci. Technol.* **26** 105023
[31] Sharma C H, Surendran A P, Varma S S and Thalakulam M 2018 *Commun. Phys.* **1** 90
[32] Tinkham M 1996 *Introduction to Superconductivity*, 2nd Edn. (New York: McGraw-Hill) pp. 316–322
[33] Harper F E and Tinkham M 1968 *Phys. Rev.* **172** 441
[34] Ashkin M and Gavaler J R 1978 *J. Appl. Phys.* **49** 2449
[35] Ashkin M, Gavaler J R, Greggi J and Decroux M 1984 *J. Appl. Phys.* **55** 1044
[36] Cirillo C, Prischepa S L, Salvato M, Attanasio C, Hesselberth M and Aarts J 2005 *Phys. Rev. B* **72** 144511
[37] Takezawa N, Koyama T and Tachiki M 1993 *Physica C* **207** 231
[38] Cooley L D and Hawes C D 1999 *J. Appl. Phys.* **86** 5696
[39] Attanasio C, Coccorese C, Mercaldo L V, Salvato M, Maritato L, Lykov A N, Prischepa S L and Falco C M 1998 *Phys. Rev. B* **57** 6056
[40] Schneider T and Schmidt A 1993 *Phys. Rev. B* **47** 5915